International Journal of Hydrogen Energy 63 (2024) 657–667

Contents lists available at ScienceDirect

International Journal of Hydrogen Energy

journal homepage: www.elsevier.com/locate/he

Effect of electrochemical charging on the hydrogen embrittlement susceptibility of a low-alloyed tempered martensitic steel submitted to high internal pressure

L.B. Peral [a,*], A. Díaz [b], C. Colombo [c], J. Alegre [b], I.I. Cuesta [b]

[a] University of Oviedo. SIMUMECAMAT Research Group, Escuela Politécnica Superior de Ingeniería de Gijón, 33203, Gijón, Spain
[b] University of Burgos, Hydrogen Technologies Research Laboratory (H2Lab), Escuela Politécnica Superior, Avenida Cantabria s/n, 09006, Burgos, Spain
[c] Politecnico di Milano, Department of Mechanical Engineering, Via La Masa 1, 20156, Milano, Italy

ARTICLE INFO

Handling Editor: Dr. E.A. Veziroglu

Keywords:
Hydrogen embrittlement
Electrochemical permeation
Cathodic hydrogen precharge
High internal pressure
Fracture micromechanisms

ABSTRACT

The influence of hydrogen on the mechanical behavior of a quenched and tempered 42CrMo4 steel has been evaluated by means of high internal pressure fracture tests carried out on hydrogen precharged notched cylindrical specimens. The notched cylindrical specimens were precharged for 3 h time with 1.2 mA/cm^2 in two different aqueous media: 1 M H_2SO_4 added with 0.25 g/l As_2O_3 and 3.5% of NaCl solution. Hydraulic fracture tests were performed at different ramps of pressure: 7000, 220, 80, 60 and 30 MPa/h, respectively. Hydrogen damage was more marked when the acid aqueous medium (1 M H_2SO_4 + 0.25 g/l As_2O_3) was employed. In this case, a higher hydrogen concentration was introduced, leading to hydrogen decohesion micromechanisms (HEDE) near the notched region, especially when tests were performed at 60 MPa/h. Hydrogen embrittlement susceptibility is discussed in terms of the microstructural singularities and the operative fracture micromechanisms observed in each case.

1. Introduction

Quenched and tempered steels alloyed with chromium, chromium-molybdenum or chromium-molybdenum-vanadium have been widely used to build pressure vessels used in the petrochemical industry. Nevertheless, hydrogen dissolved in low-alloyed steels can drastically influence their mechanical properties leading to hydrogen embrittlement (HE) phenomenon. HE is dependent on several factors such as hydrogen-charging methodology or loading rate. Hence, the degree of susceptibility of materials to HE influences their selection to work safely in a hydrogen atmosphere.

During last years, many studies have been carried out to analyze the effect of hydrogen on the mechanical properties of low-alloyed martensitic steels. In this regard, Matsunaga et al. [1] studied the effect of hydrogen in a quenched and tempered Cr–Mo steel (σ_{ys} = 671 MPa) by slow strain rate tensile in-situ tests (0.12 mm/min). They reported a marked reduction in ductility after testing in hydrogen gas under a pressure of 115 MPa. On the other hand, Peral et al. [2] also studied the influence of hydrogen in different quenched and tempered Cr–Mo–V steel grades (σ_{ys} = 430–761 MPa) by slow strain rate tensile ex-situ tests. In this study, hydrogen-precharged notched samples were used. Hydrogen damage was mainly observed at the lowest displacement rates (0.0004 mm/min) and it was especially clear in the V-free grades. V. Arniella et al. [3] analyzed hydrogen effect on tensile properties of a tempered 42CrMo4 steel (σ_{ys} = 622 MPa) by means of ex-situ and in-situ tests at different displacement rates. An important reduction of the tensile strength was noted, especially, when notched specimens were subjected to in-situ electrochemical H-charging in an acid aqueous medium. The same grade of steel was also employed by G. Álvarez et al. [4] to study the influence of current density and displacement rate on hydrogen embrittlement susceptibility by means of electrochemical in-situ small punch tests. Hydrogen damage susceptibility increased as displacement rate decreased and the applied current density increased.

Furthermore, hydrogen influence on fracture toughness of Cr–Mo steels has been also widely studied through the literature. A. Zafra et al. [5] evaluated the influence of tempering time on the fracture toughness of hydrogen pre-charged 42CrMo4 steel. The fracture toughness is reduced due to internal hydrogen and HE increased when the tempering time decreased. A similar study was also conducted in Ref. [6]. Peral et al. [7] also analyzed the effect of hydrogen on fracture toughness of

* Corresponding author.
E-mail address: luisborja@uniovi.es (L.B. Peral).

https://doi.org/10.1016/j.ijhydene.2024.03.034
Received 26 December 2023; Received in revised form 24 February 2024; Accepted 3 March 2024
Available online 21 March 2024

Table 1
Chemical composition (weight %).

Fe	C	Mn	Si	Cr	Mo
bal.	0.42	0.62	0.18	0.98	0.22

Cr–Mo–V steel grades, using CT specimens thermally pre-charged with hydrogen gas. In accordance with [6], they also reported that HE was also found to be much greater in the Cr–Mo grades tempered at the lowest temperatures. Besides, in the V-added grade, the presence of hydrogen did not modify the failure micromechanims. In this regard, sub-micrometric vanadium carbides [8] precipitated during the tempering treatment act as strong hydrogen trapping sites, relieving hydrogen damage [9]. In this respect, the effect of 'hydrogen trapping' plays an important role in the hydrogen embrittlement process. Hydrogen atoms are known to be retained in tempered martensite microstructures at microstructural traps, such as prior austenitic grain boundaries, martensitic laths, block and packet interfaces, dislocations, matrix-precipitated carbide interfaces and matrix-inclusion interfaces [2,10–12].

Regarding the influence of hydrogen on the fatigue crack growth rate (FCGR) of Cr–Mo steels, L. Briottet et al. [13] evaluated the fatigue crack initiation and growth on a low alloy quenched and tempered Cr–Mo steel ($\sigma_{ys} = 630$ MPa) under hydrogen pressure in the range 0.5–35 MPa (in-situ tests). They found that the effect of hydrogen on the fatigue crack growth rate depends on the stress intensity factor amplitude (ΔK) and gas pressure. At low ΔK and pressures lower than 0.5 MPa, the effect of hydrogen was negligible whereas FCGR notably increased at 10 MPa H_2. However, at higher ΔK values, the FCGR increased, even at low pressure. On the other hand, Murakami et al. [14] studied the effect of internal hydrogen, by ex-situ tests, in the FCGR of a Cr–Mo steel JIS SCM435. Hydrogen damage was more pronounced for the lowest ΔK values and FCGR especially increased with decreasing test frequency. At higher value of ΔK, hydrogen-charged samples gradually merge to the line of the uncharged samples, because the crack propagates much faster than hydrogen diffusion to the crack tip. This behavior was clearly reported in Ref. [15]. Despite many studies have analyzed the influence of hydrogen in the FCGR [16–20], a recent work [21] has evidenced that FCGR is notably marked (even at higher ΔK values) when experiments are carried out in a hydrogen gas atmosphere (in-situ) in comparison to FCGR results obtained using hydrogen-precharged samples (ex-situ).

The use of hydraulic fracture tests at high internal pressure to characterize hydrogen embrittlement is scarce in the literature. The novelty of this work consists on analyzing hydrogen embrittlement behavior by using very small tubular specimens with an axial notch in a 42CrMo4 tempered martensitic steel intended to work in a hydrogen environment. The unique design of experiment for hydrogen embrittlement allows to reduce the volume of the material to test and, applying an inner pressure, we can reproduce a stress state similar to the operative condition of a pipeline. Besides, to evaluate hydrogen damage, five different loadings rates were applied: 7000, 220, 80, 60 and 30 MPa/h in order to study the interaction between strain rate and hydrogen transport kinetics towards the notch tip region. Finally, in order to validate two different experimental methodologies and assess if they are comparable, hydrogen uptake and diffusion have been characterized by means of room temperature desorption curves and electrochemical permeation experiments.

2. Material

A low-alloyed ferritic steel (42CrMo4 grade, AISI4140) has been employed in this study. The chemical composition is given in Table 1.

Hot-rolled plates of 250 × 250 × 12 mm^3 were austenitized at 845°C for 45 min, quenched in water and finally, tempered at 700°C for 2 h. The obtained microstructure is given in Fig. 1. It mainly consists of highly tempered martensite with prior austenite grain size (PAGS) 20 ± 5 μm and hardness 207HV_{30}. The profuse (Fe,Cr)C precipitation [22] that takes place during the tempering treatment at 700 °C can be clearly observed in a tempered martensitic matrix (Fig. 1(b)). For more details regarding the microstructural features, the reader is addressed to Ref. [23].

The present work analyses the same material, manufacturing process and heat treatment than reference [24]. Therefore, mechanical properties in the absence of hydrogen are extracted from tensile testing in that study and shown in Table 2. HV is the Vickers hardness, σ_{ys} represents the yield strength, σ_{uts} the ultimate tensile strength and A is the elongation at fracture.

3. Experimental procedure

3.1. Hydrogen electrochemical precharge

To evaluate hydrogen embrittlement susceptibility, hydrogen was electrochemically precharged at room temperature (~ 21°C) with a current density of 1.2 mA/cm^2 for 3h, Fig. 2. The current density was chosen with the same value for precharging and for permeation testing to facilitate the interpretation of diffusion effects, and it is slightly higher than in other studies [3,4] in order to ensure saturation after 3 h. Additionally, the value of 1.2 mA/cm^2 has been previously used to study hydrogen embrittlement of notched cylindrical samples [22]. Two different aqueous media were employed: 1 M H_2SO_4 added with 0.25 g/l As_2O_3 (pH ~ 1) and 3.5% of NaCl (pH ~ 6.7). Moderated agitation was employed during the hydrogen precharging process. Similar hydrogen charging conditions have been successfully employed in Refs. [3,22] to evaluate HE susceptibility in a quenched and tempered martensitic steel. The experimental set up is shown in Fig. 2.

Table 2
Conventional mechanical properties [24].

HV_{30}	σ_{ys} (MPa)	σ_{uts} (MPa)	A (%)
207	622	710	23

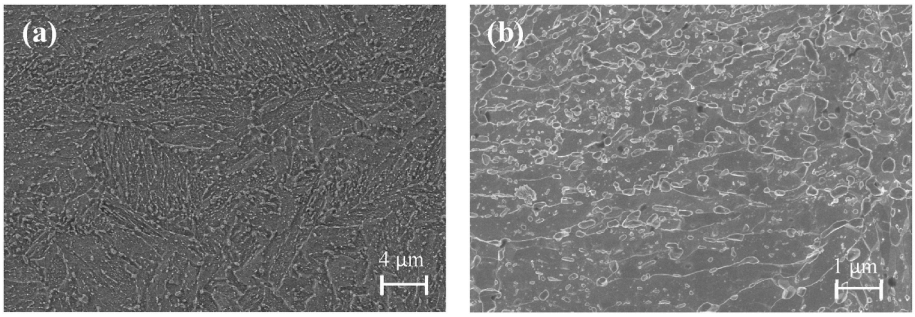

Fig. 1. 42CrMo4 microstructures at different magnification (etched with Nital-2%.). (a) 2500x and (b)10000x

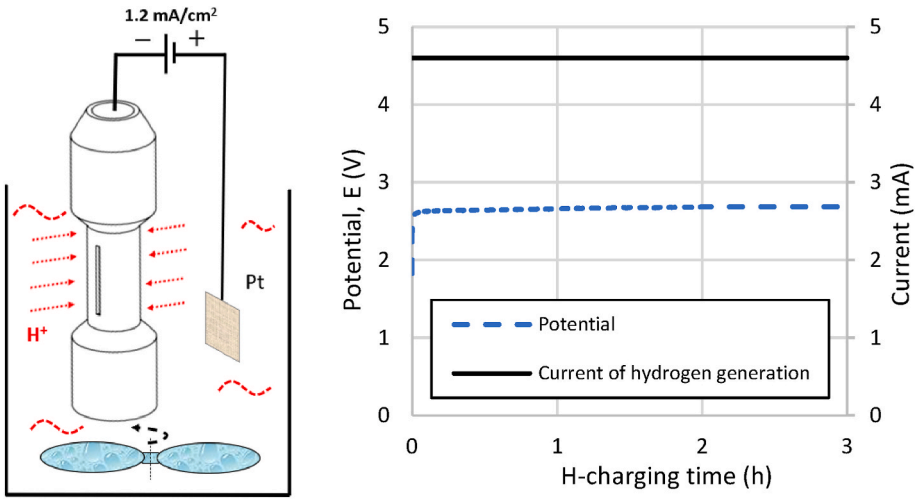

Fig. 2. Experimental set up and hydrogen precharging conditions.

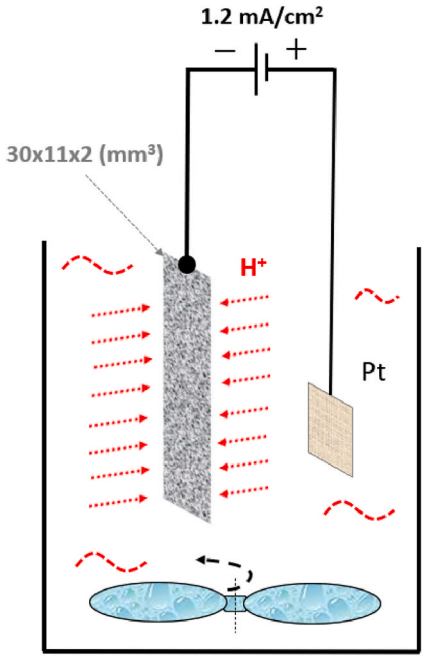

Fig. 3. Hydrogen precharging of thin plates (2 mm thickness) to conduct desorption curves at room temperature (RT).

3.2. Hydrogen desorption curves and electrochemical hydrogen permeation tests

In order to evaluate the hydrogen diffusion kinetics, thermal desorption tests and electrochemical permeation experiments were conducted. Plates of 30 mm length, 11 mm width and 2 mm thickness were machined to analyze hydrogen desorption at room temperature. Thin plates were cathodically charged in a 1 M H_2SO_4 + 0.25 g/l As_2O_3 and 3.5% of NaCl solution with 1.2 mA/cm^2 for 3 h time (Fig. 3).

After H-precharging, the introduced hydrogen concentration was measured by hot extraction with a LECO DH603 analyser, maintaining the thin plates at 1100 °C for 300 s. Additionally, some of the charged thin plates in the acid aqueous solution (pH ~ 1) were also exposed to air for different intervals of time: 2, 4 and 24 h, respectively. Diffusivity and trapping features are fitted from the experimental desorption curve at room temperature, considering two different numerical approaches based on the finite element method (FEM), as described in Ref. [22].

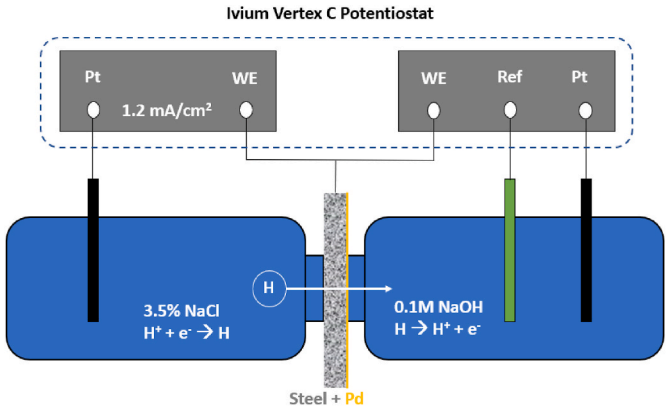

Fig. 4. Electrochemical hydrogen permeation. WE is the working electrode, Ref is the reference electrode and Platinum (Pt) was used as a counter electrode.

Permeation experiments were conducted in 3.5% of NaCl in order to compare hydrogen uptake and diffusion features with those obtained from the thermal desorption curves. Hence, hydrogen absorption, permeation and diffusion were also studied using the electrochemical double cell that was first proposed by Devanathan and Stachurski [25]. Hydrogen atoms were generated on the charging cell and the diffusing hydrogen atoms were oxidized on the anodic cell, corresponding to the exit side. An anodic current density was continuously recorded using an Ivium Vertex C potentiostat. On the entry side, hydrogen was generated under a current density of 1.2 mA/cm^2 using a 3.5% of NaCl medium with a pH ~ 6.7. A circular area of approximately 1 cm^2 was exposed to the solution and the electrochemical tests were conducted at room temperature on samples with 1 mm thickness. The anodic cell contained 0.1 M NaOH solution with a pH ~ 12. Before carrying out permeation experiments, sample surface facing the exit side of the double-cell was electrolytically coated with a Je42V palladium solution that contained 0.2 g/l Pd. Electroplating was performed by applying a current density of 3 mA/cm^2 for 600 s and moderated agitation was employed during the electroplating. Similar conditions were previously employed in Refs. [2,26]. Thereupon, the sample was immediately placed into the double-cell and the Open Circuit Potential (OCP) was monitored in 0.1 M NaOH solution until potential stabilized. Then, the exit side was polarized to the final potential monitored during the OCP measurement, −50 mV, after stabilizing. This potential was considered enough to facilitate hydrogen oxidation [2,26]. Besides, the anodic current density, on the exit side, could be also stabilized and maintained around

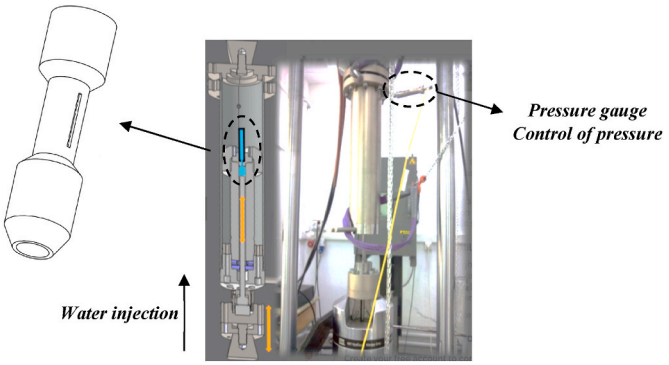

Fig. 5. Experimental set-up. Hydraulic fracture test device.

0.15 μA/cm^2 [27] before performing the galvanostatic hydrogen cathodic charging, with 1.2 mA/cm^2 in 3.5% of NaCl. Fig. 4 displays the schematic Devanathan-Stachurski double cell employed in this study.

Apparent diffusivity (D_{app}), apparent permeability (P_{app}) and the apparent hydrogen concentration (C_{app}) were calculated according to Ref. [27].

3.3. High internal pessure hydraulic fracture tests

Hydraulic fracture tests have been carried out in a high-pressure test device (Fig. 5) that is able to attain 6000 bar of internal pressure. The H-precharged notched miniature specimens were located in a MTS820. High-internal pressure was automatically applied, injecting water by means of the piston, towards the interior of the miniature specimens at different ramps of pressure: 7000, 220, 80, 60 and 30 MPa/h.

Fig. 6 shows the geometry of the notched cylindrical specimens employed in this study. A longitudinal notch of 250 μm depth, 60° angle and tip radius less than 0.1 mm was machined. The ideal ligament length is of 250 μm.

3.4. Numerical modelling of stress concentration

Stress-driven hydrogen accumulation around the notch tip region is expected to play a critical role in the hydrogen embrittlement phenomenon.

The hydrostatic stress distribution is numerically determined using the commercial finite element software ABAQUS Standard. 2D quadrilateral second-order elements with reduced integration are used and plane strain conditions are assumed. A half of the cross section is simulated because of symmetry, and the corresponding boundary conditions are imposed, i.e. the displacement perpendicular to the symmetry axis is restricted. Loading is modelled through a pressure on the inner surface, and the considered material behaviour follows a power-law hardening with the yield stress from Table 2 and a hardening exponent of 0.12 [24]. Young's modulus is taken as E = 210 GPa and the Poisson's coefficient $\nu = 0.3$.

3.5. Observation of fracture surfaces

Fracture surfaces of the fracture-tested cylindrical specimens were carefully observed in a scanning electron microscope, JEOL JSM-6460LV, using an acceleration voltage of 20 kV.

4. Results and discussion

4.1. Thermal desorption analysis and electrochemical hydrogen permeation

Hydrogen content was measured by means of a LECO DH603 hydrogen analyser. Fig. 7 displays the thermal desorption profiles obtained by hot extraction in the 42CrMo4 grade, after hydrogen precharging with 1.2 mA/cm^2 for 3 h in 1 M H_2SO_4 + 0.25 g/l As_2O_3 and 3.5% NaCl solution, respectively. Hydrogen content introduced in 1 M

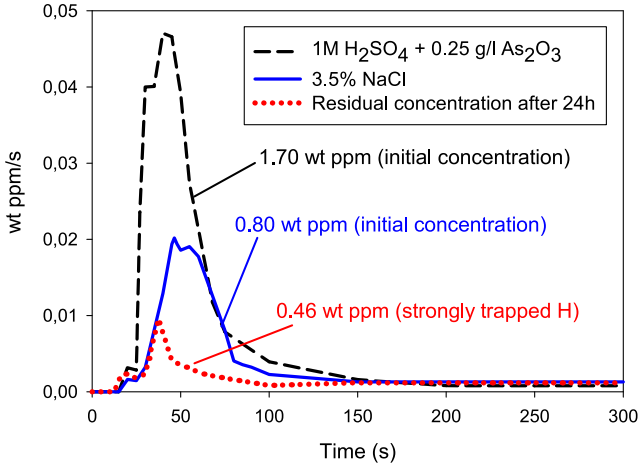

Fig. 7. Measured hydrogen concentration in thin plates of a 42CrMo4 steel as a function of the precharging media. Hot extraction at 1100°C for 300s.

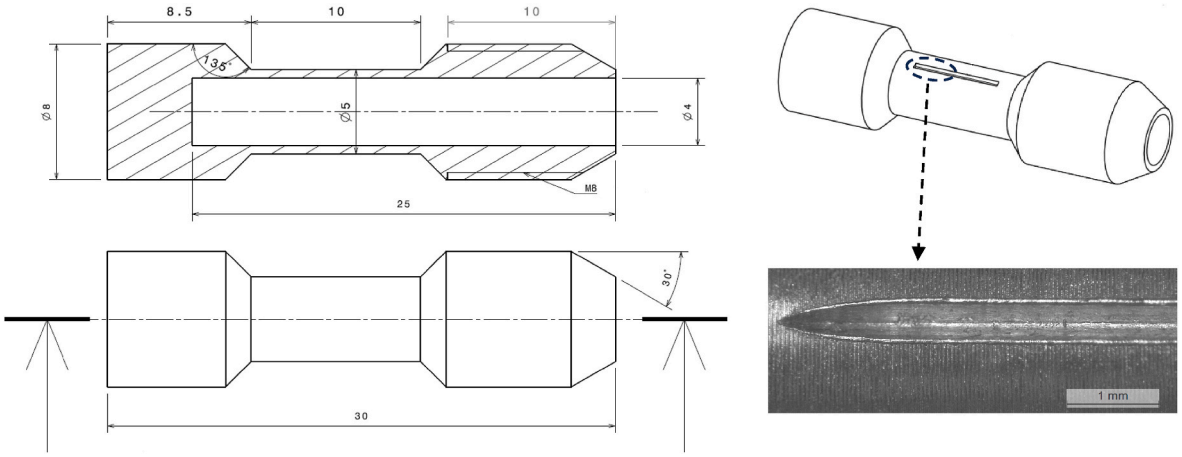

Fig. 6. Notched-miniature cylindrical specimen (dimensions in mm).

Table 3
Interaction hydrogen-microstructure. Results obtained after hydrogen precharging in the acid aqueous solution.

Hydrogen desorption curve (Fig. 8)			Finite element analysis (FEM in Fig. 8)		
C_0 (wt ppm)	$C_{residual}$ (wt ppm)	C_{dif} (wt ppm)	D_{app} (m^2/s)	N_T (sites/m^3)	E_b (kJ/mol)
1.70	0.46	1.24	$3{\cdot}10^{-11}$	$5{\cdot}10^{24}$	45

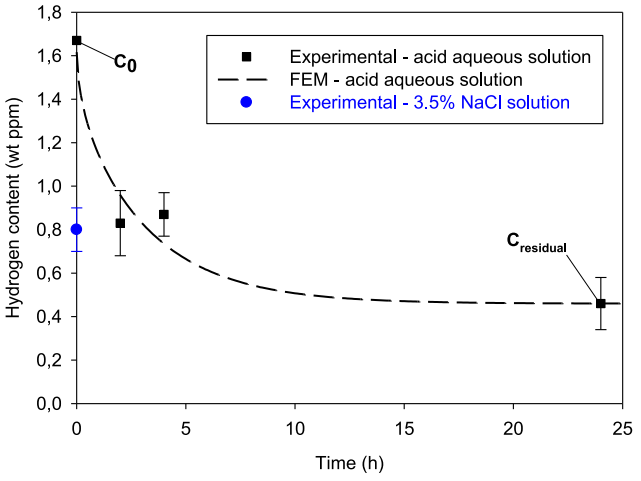

Fig. 8. Hydrogen desorption curve at RT after hydrogen charging in the acid aqueous solution. Blue point corresponds to the initial hydrogen content introduced after H-charging in 3.5% of NaCl. (For interpretation of the references to colour in this figure legend, the reader is referred to the Web version of this article.)

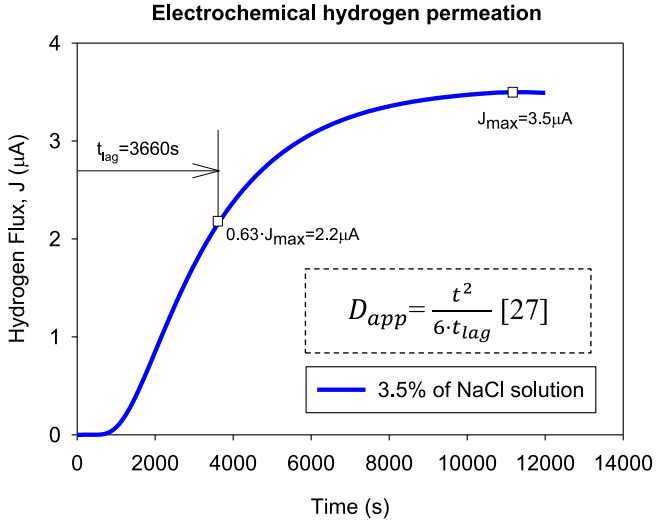

Fig. 9. Electrochemical permeation tests in 3.5% of NaCl with 1.2 mA/cm.^{2}.

H_2SO_4 + 0.25 g/l As_2O_3 was 1.70 wt ppm whilst hydrogen concentration decreases to 0.80 wt ppm in 3.5% of NaCl. This fact can be explained due to the higher hydrogen recombination in the surface of the steel when hydrogen charging is conducted in 3.5% of NaCl [28]. It is important to mention that before precharging, hydrogen content was determined to be 0.3 wt ppm.

In order to analyze hydrogen desorption kinetics at room temperature, some of the thin plates were exposed to air, after hydrogen precharging, for 2, 4 and 24 h. Hence, the apparent diffusivity (D_{app}), the density of traps (N_T) and the binding energy (E_b) were calculated (Table 3) by the data fitting carried out from the experimental hydrogen desorption curve (Fig. 8). The introduced hydrogen concentration, C_0, corresponds to the first point of the curve (t = 0) while $C_{residual}$ is the hydrogen concentration that is strongly trapped in the microstructure, after a long exposure at room temperature (24h in this study). Diffusible hydrogen (C_0 – $C_{residual}$) is the amount that is able to escape from microstructural traps (C_{dif}). These values are also summarized in Table 3.

Table 4
Electrochemical permeation results in 3.5% of NaCl solution calculated according to [27].

Electrochemical permeation (Fig. 9) with 1.2 mA/cm^2		
D_{app} (m^2/s)	C_{app} (wt ppm)	P_{app} (molH/m·s)
$3.8\ (\pm\ 0.75){\cdot}10^{-11}$	1.2 (± 0.25)	$2{\cdot}10^{-10}$

On the other hand, the apparent diffusion coefficient (D_{app}) was also determined by the electrochemical hydrogen permeation experiments (Fig. 9) performed, in this case, in 3.5% of NaCl solution. A D_{app} of $3.8{\cdot}10^{-11}$ m^2/s was obtained from the t_{lag} method [27]. This value is quite similar to that determined by the numerical fitting of the desorption curve ($3{\cdot}10^{-11}$ m^2/s, Table 3) after hydrogen precharging in 1 M H_2SO_4 + 0.25 g/l As_2O_3 (acid aqueous medium).

Therefore, this fact contributes to justify that trapping and detrapping kinetics in the steel microstructure of the quenched and tempered 42CrMo4 steel grade is mainly dominated by hydrogen trapping sites regardless of the hydrogen charging solution. Results extracted from the permeation experiments are given in Table 4, where D_{app} is the apparent diffusivity, C_{app} represents the apparent hydrogen concentration and P_{app} is the apparent permeability.

According to the results, it could be also verified that the apparent hydrogen concentration (i.e. subsurface hydrogen concentration in the hydrogen generation side) is also similar to that introduced from the hydrogen charging solution (∼ 0.8 wt ppm) in 3.5% of NaCl, with 1.2 mA/cm^2 for 3 h (Fig. 7).

On the other hand, the density of trapping sites (N_T) was found to be $5{\cdot}10^{24}$ sites/m^3. Similar values of N_T have been reported in Refs. [11,29] for quenched and tempered microstructures. Regarding the binding energy, E_b ∼ 45 kJ/mol, could be mainly associated to hydrogen trapped along the high angle grain boundaries [30,31]. It should be recalled that in quenched and tempered microstructures, dislocations re-arranged in cells and these cell interfaces also correspond to lath, packet and block martensitic interfaces and its interaction to the PAGB. Here, most carbides also precipitate, and thus it is very difficult to separate the trapping contribution from all these different microstructural features. According to Ref. [32], hydrogen trapping by high angle grain boundaries (HAGBs) was confirmed by TDS with a binding energy of 44.7 kJ/mol, similar to that found in this work. Despite this, it is clear that this hydrogen trapped also includes trapped hydrogen at vacancies and dislocations accumulated at HAGBs [33].

4.2. Hydraulic fracture tests

Fig. 10 displays the variation of the pressure recorded as a function of the time for the uncharged and hydrogen precharged notched specimens, tested in 1 M H_2SO_4+0.25 g/l As_2O_3 and 3.5% of NaCl, respectively. The burst pressure (P_b) and the embrittlement indexes (EI) are shown in Table 5. Besides, Fig. 11 gives the burst pressure variation as a function of the applied ramp of pressure in both hydrogen precharging media. As can be observed, hydrogen effect has been mainly marked at 60 MPa/h after 1.5h testing time, because the reached pressure peak is lower.

The general fracture surface corresponding to the uncharged condition is shown in Fig. 12(a). Fig. 12(b) and (c) show the fracture surface

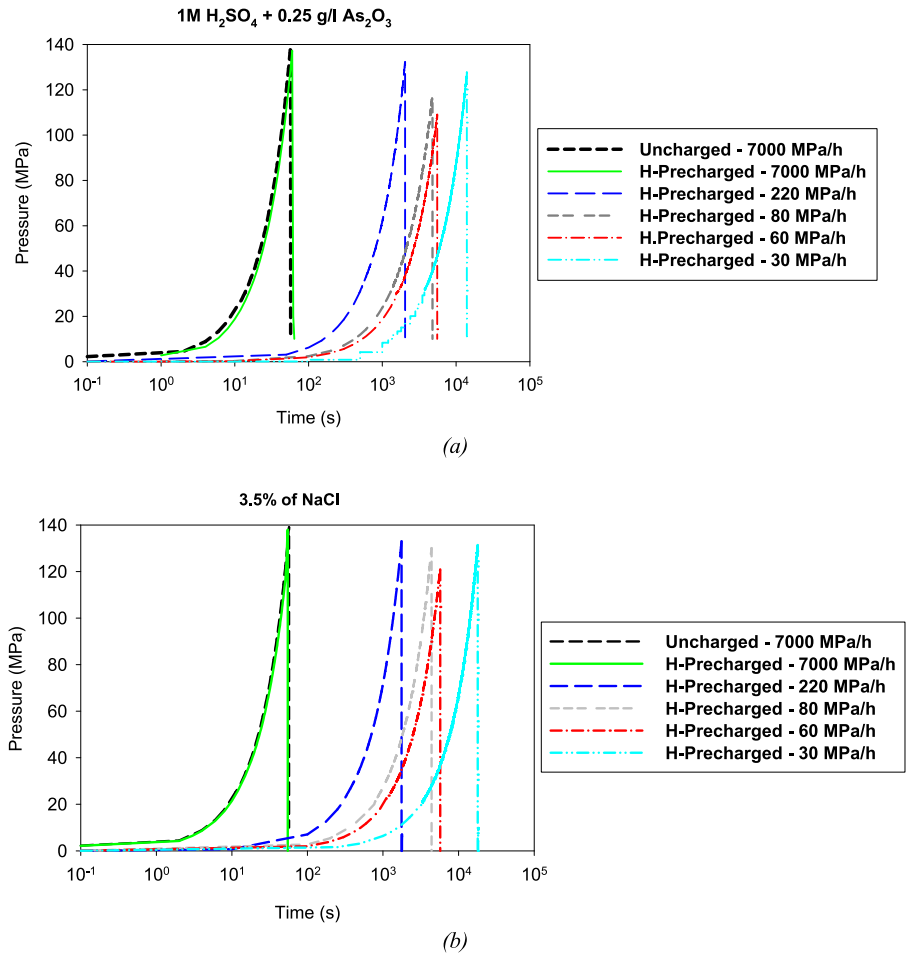

Fig. 10. Hydraulic fracture tests curves at high internal pressure. (a)1 M H_2SO_4 + 0.25 g/l AS_2O_3 and (b) 3.5% of NaCl solution.

Table 5
Hydraulic fracture tests results and embrittlement indexes (EI in %) related to the burst pressure (P_b). Embrittlement Index: EI (%) $= \frac{X_{no-H} - X_H}{X_{no-H}} \cdot 100$.

	V_{test} (MPa/h)	Hydrogen precharging solution			
		1 M H_2SO_4 + 0.25 g/l As_2O_3		3.5% NaCl	
		P_b (MPa)	EI P_b (%)	P_b (MPa)	EI P_b (%)
Uncharged	7000	137 ± 7	–	137 ± 7	–
H-precharged	7000	134	2	136 ± 3	1
	220	132	4	132 ± 2	4
	80	118 ± 5	12	130 ± 5	5
	60	109 ± 6	19	120 ± 4	12
	30	128 ± 3	5	131 ± 5	4

after precharging and testing in 1 M H_2SO_4 + 0.25 g/l As_2O_3 and 3.5% NaCl, respectively. In both cases, fracture surface corresponds to the samples tested at 60 MPa/h, i.e. the maximum embrittlement level.

According to these results, hydrogen embrittlement was more pronounced in the hydraulic fracture tests carried out with hydrogen precharged samples into the acid solution (1 M H_2SO_4 + 0.25 g/l As_2O_3). In this case, the operative fracture micromechanism changed in the presence of internal hydrogen, especially at 60 MPa/h (Fig. 13 –left side). In the uncharged specimens, the fracture micromechanism always consisted in the initiation, growth and coalescence of microvoids (MVC). Nevertheless, in the specimen tested at 60 MPa/h after hydrogen precharging into the acid solution (pH ~ 1), a region near the notch with the

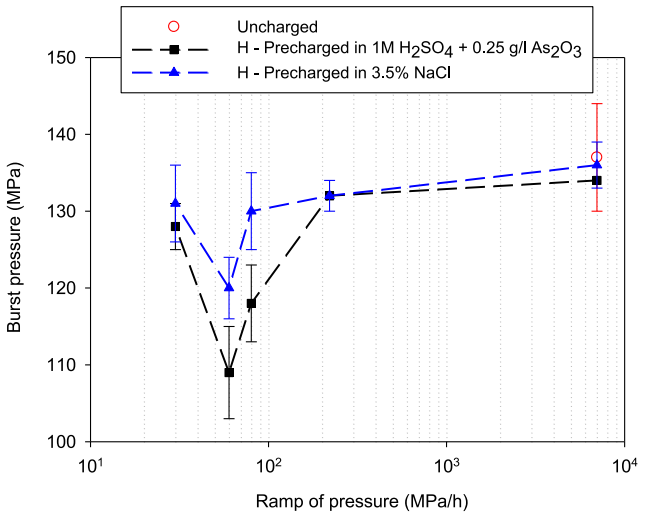

Fig. 11. Burst pressure trend as a function of the applied ramp of pressure.

appearance of a quasi-cleavage (QC) was clearly observed. In this region, very small dimples, which correspond to the carbide-matrix interfaces decohesion [24], were also observed to 125 μm from the notch. The average size of these small dimples is ~ 500 nm. (Fe,Cr)C precipitated during the tempering treatment at 700°C can range from 500 to

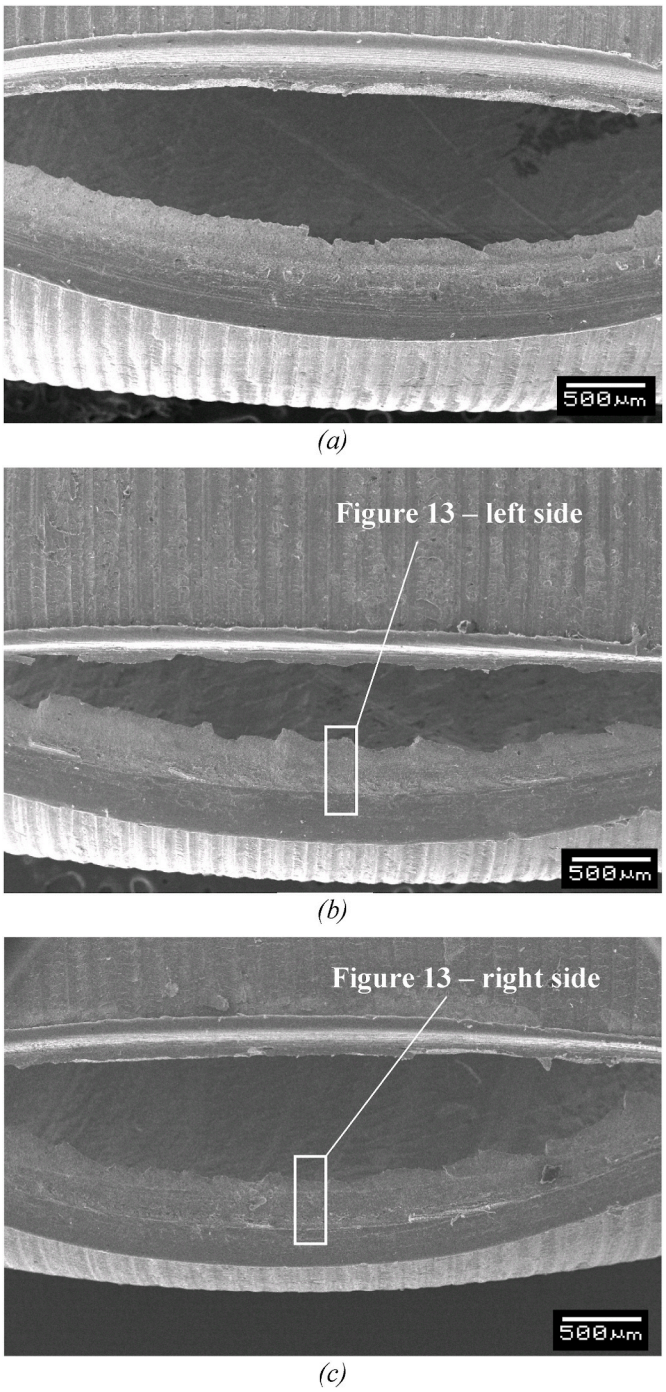

Fig. 12. General fracture surfaces. (a) Uncharged sample. (b) Hydrogen precharged and tested at 60 MPa/h in 1 M H_2SO_4 + 0.25 g/l As_2O_3 and (c) Hydrogen precharged and tested at 60 MPa/h in 3.5% NaCl. In Fig. 12(b) and (c) are indicated the areas analyzed at higher magnification in Fig. 13.

1000 nm [23] that is comparable to the size of small dimples (i.e. carbide-matrix interfaces decohesion), noted within the first 125 µm, from the notch. However, at 220 and 30 MPa/h, CMD micromechanism was not especially pronounced, even near the notched region.

After hydrogen precharging in 3.5% of NaCl and testing, hydrogen micromechanism was barely modified and MVC was always the main operative fracture micromechanism (Fig. 13 – right side) and regardless of the applied loading rate (MPa/h). However, in the 3.5% NaCl condition at 60 MPa/h, a brittle region is observed near the notch surface (Fig. 13d). In contrast to results for the H_2SO_4 electrolyte, the CMD mechanism in which smaller dimples nucleated due to carbide-matrix decohesion, is not observed near the region at approximately 125 µm from the notch tip. Despite the 3.5% NaCl condition produces MVC at all the displacement rates, hydrogen reduces the critical dimple size for void coalescence and produces a quasi-cleavage appearance. This mechanism results in an embrittlement index around 12% at 60 MPa/h, comparable to the index at 80 MPa/h in the acid solution, indicating that the hydrogen-accelerated void coalescence can be as critical as CMD processes. The absence of CMD is explained by the lower concentration after pre-charging in the NaCl solution, which is enough to trigger very localized quasi-cleavage at the notch tip but not enough for carbide/matrix interface cracking.

It is also important to mention that embrittlement indexes (EI) trend decreased when mechanical tests were carried out at 30 MPa/h. In this situation, testing time was higher than 4 h and consequently, part of diffusible hydrogen could have already diffused out of the samples during the hydraulic fracture test, relieving the embrittlement phenomenon. If we take into consideration, results previously given in Fig. 8, using hydrogen precharged samples, test duration should be limited to no more than 5h. After that time, hydrogen remains strongly trapped (at RT) in the steel microstructure ($C_{residual} \approx 0.46$ wt ppm). Several authors have argued that irreversible hydrogen, strongly trapped, is not at the origin of the mechanical deleterious associated with hydrogen embrittlement [2,34]. At 30 MPa/h, the loss of hydrogen at RT seems to prevail because the loading rate (very low in this case) and the apparent diffusivity (high for this test condition) are not well coupled to keep promoting hydrogen damage. Taking as a reference the results previously given in Fig. 7, hydrogen concentration introduced after hydrogen precharging into the acid medium (~ 1.7 wt ppm) was notably higher than that introduced into the 3.5% of NaCl solution (~ 0.8 wt ppm). This fact contributes to justify the highest embrittlement indexes found after hydrogen precharging in 1 M H_2SO_4 + 0.25 g/l As_2O_3.

When a notched component is submitted to an external load (i.e. high internal pressure) in the presence of hydrogen, hydrogen atoms can diffuse through the microstructure and accumulate at the stress concentration region (Fig. 14) located in front of the notch [35]. According to this, hydrogen concentration in the vicinity of a notch ($C_{H,notch}$) is dominated by hydrostatic stress (σ_H) and can be estimated by **equation (1)** [36].

$$C_{H,notch} = C_{dif}\ exp\left(\frac{\sigma_H \cdot V_H}{R \cdot T}\right) \quad (1)$$

In order to explain the induced hydrogen damage after precharging in both hydrogenated media, hydrogen concentration in the vicinity of the notch was calculated at the moment of failure, only for the maximum embrittlement level, at 60 MPa/h. Hence, hydrostatic stress profiles given in Fig. 14 corresponds to hydrostatic stress distribution to an inner hydraulic pressure of 120 MPa (burst pressure for the 3.5% NaCl condition at 60 MPa/h) and 109 MPa (burst pressure for the acid solution at 60 MPa/h), respectively. Also in **equation (1)**, C_{dif} is the hydrogen content that is able to diffuse through the steel microstructure and it has been estimated from the hot extraction analysis (Fig. 7). To determine diffusible hydrogen for the 3.5 % NaCl charging condition ($C_0 - C_{residual}$), the residual concentration was assumed to be the same as in 1 M H_2SO_4 + 0.25 g/l As_2O_3, i.e. 0.46 wt ppm measured from the room temperature desorption curve (Fig. 8). Despite the 3.5% NaCl charging condition introduces lower concentrations (0.80 wt ppm, as shown in Fig. 7), this level is higher than the residual concentration and therefore traps can be assumed as saturated, and the simplification is reasonable.

In the same equation, V_H represents the partial molar volume of hydrogen in BCC iron ($V_H = 2.1 \cdot 10^{-6}$ m^3/mol), R is the gas constant (8.31 J/molK) and T is the testing temperature (20°C). The maximum hydrostatic stress at the moment of failure (at 60 MPa/h), the diffusible hydrogen content (C_{dif}) and the hydrogen concentration accumulated in the notch tip ($C_{H,notch}$) are given in Table 6.

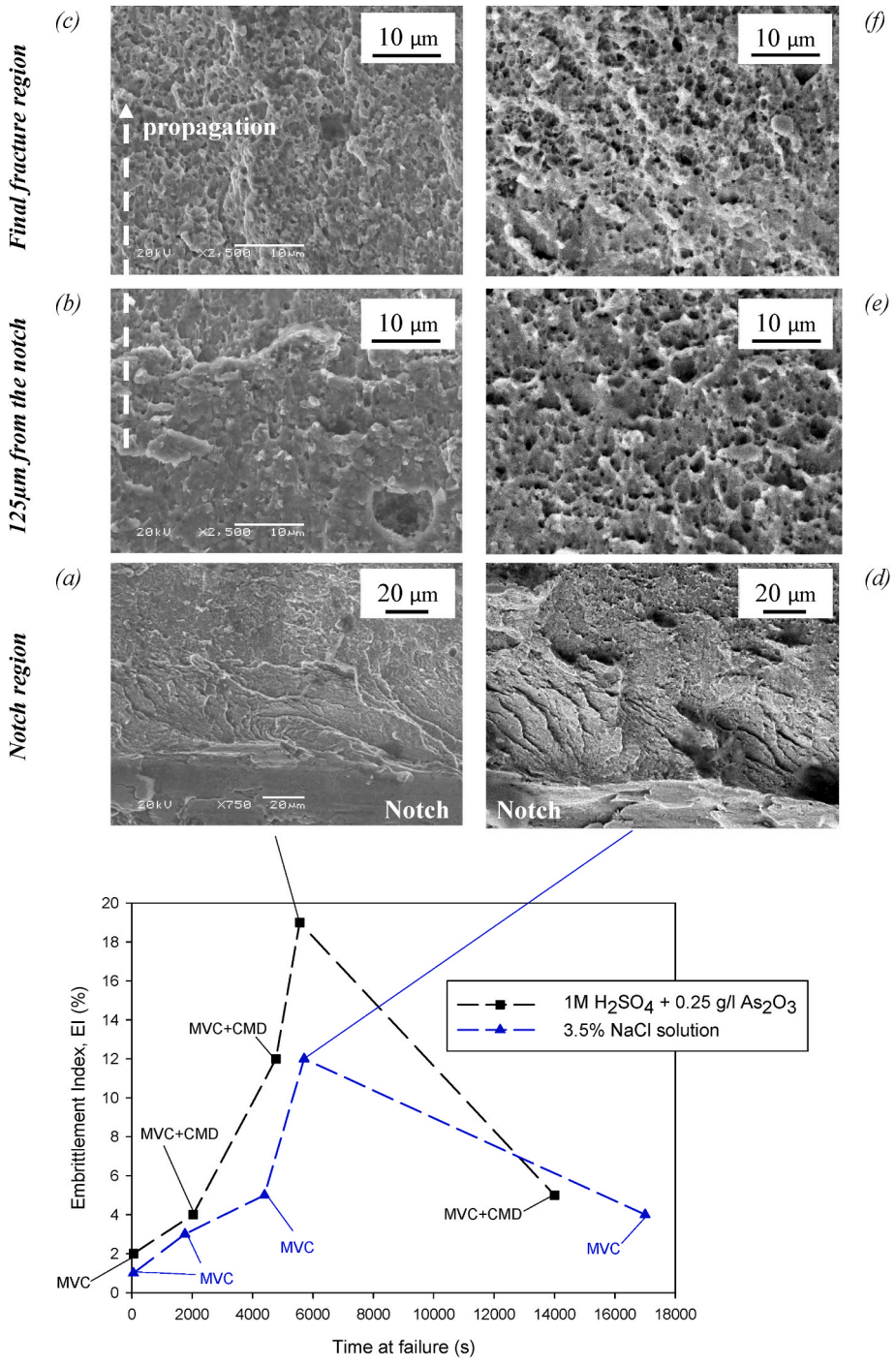

Fig. 13. Average embrittlement indexes trend and fracture micromechanisms. (a)(b)(c) Tests at 60 MPa/h after precharging in 1 M H_2SO_4+0.25 g/l As_2O_3 solution and (d)(e)(f) Tests at 60 MPa/h after precharging in 3.5% of NaCl. MVC: microvoids coalescence and CMD: carbides matrix interfaces decohesion.

Hence, after hydrogen precharging into the acid solution and especially at 60 MPa/h equivalent to 1.5 h testing time, a critical hydrogen content ~ 2.60 wt ppm is reached in the notched area. Under this test condition, loading rate and apparent diffusivity ($3{\cdot}10^{-11}$ m^2/s) seem to be now coupled, and hydrogen atoms have time enough to attain the notched region by virtue of its diffusion coefficient, leading to a high level of embrittlement (EI ~ 19%, Fig. 13). Unlike what has been observed after hydrogen precharging in 3.5% of NaCl, the mentioned critical hydrogen concentration was able to trigger decohesion micromechanisms (QC + CMD, Fig. 13– left side). According to Refs. [37–39], we postulate that the enhancement of dislocation activity caused by the hydrogen enhanced localized plasticity (HELP) mechanism promotes hydrogen transport by dislocations. In this regard, an enhancement in the hydrogen-transported by dislocations is expected after hydrogen precharging in the acid aqueous solution because of the higher hydrogen uptake (~ 1.70 wt ppm, Fig. 7). Therefore, quasi-cleavage (QC) happens due to the local hydrogen enrichment in the vicinity of the notch (2.6 wt ppm, Table 6 at 60 MPa/h). In quenched and tempered steels, this fracture morphology is known as plasticity related hydrogen induced cracking, PRHIC [40]. It is described as a fracture surface characterized by ductile micro-plastic tearing on a very fine scale, along the martensitic lath, block and packets interfaces. Definitely, decohesion mechanisms (HEDE) are induced when these tempered martensitic interfaces suffer an additional hydrogen enrichment due to hydrogen

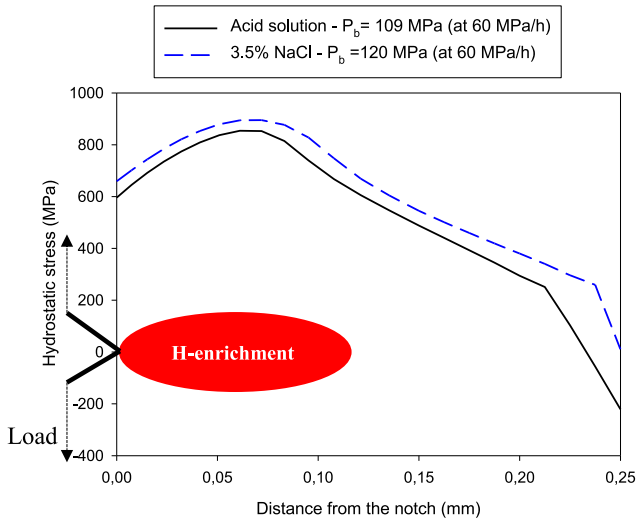

Fig. 14. Hydrostatic stress distribution in the vicinity of the notch at the moment of failure at 60 MPa/h of internal pressure (maximum embrittlement, Fig. 11).

Table 6
Critical hydrogen concentration ($C_{H,notch}$) reached in the vicinity of the notch at 60 MPa/h.

Aqueous solution	P_b (MPa)	$\sigma_{H-max.}$ (MPa in Fig. 14)	C_{dif} (wt ppm)	$C_{H,notch}$ (wt ppm)
1 M H_2SO_4 + 0.25 g/l As_2O_3	137 → 109	854	1.24	2.60
3.5% of NaCl	137 → 120	895	0.34	0.74

transport by dislocations (Fig. 15) encouraged by stress concentration (high triaxiality) near the notch region. Additionally, this local hydrogen enrichment also leads to decohesion along the matrix-carbide interfaces (CMD). This hypothesis contribute to justify the decohesion micromechanisms observed in samples precharged in 1 M H_2SO_4 + 0.25 g/l As_2O_3 solution. It is also important to mention that intergranular fracture was not observed in this steel grade. In this regard, we postulate microstructure (Fig. 1) is sufficiently relaxed after tempering at 700°C and thus the grain boundary decohesion does not happen. Previous studies performed in quenched and tempered CrMo steels have revealed that intergranular fracture usually occur when the yield strength exceeds 750–800 MPa [41]. In our case, the yield strength is 622 MPa. Consequently, hydrogen distributes in a more uniform way in the microstructure with quite uniform dispersion of carbides, promoting QC (PRHIC) and CMD micromechanims, only after significant plastic deformation, in the case of the samples precharged in the acid solution.

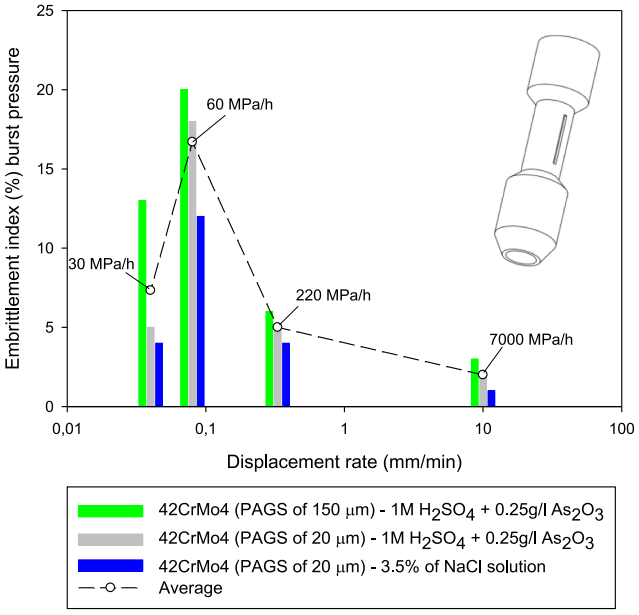

Fig. 16. *Influence of the prior austenite grain size and hydrogen charging solution in hydrogen embrittlement susceptibility analyzed by hydraulic fracture tests at high internal pressure in a 42CrMo4 steel (ex-situ tests). Results corresponding to 42CrMo4 steel with PAGS* = 150 μm *were previously published in* [22].

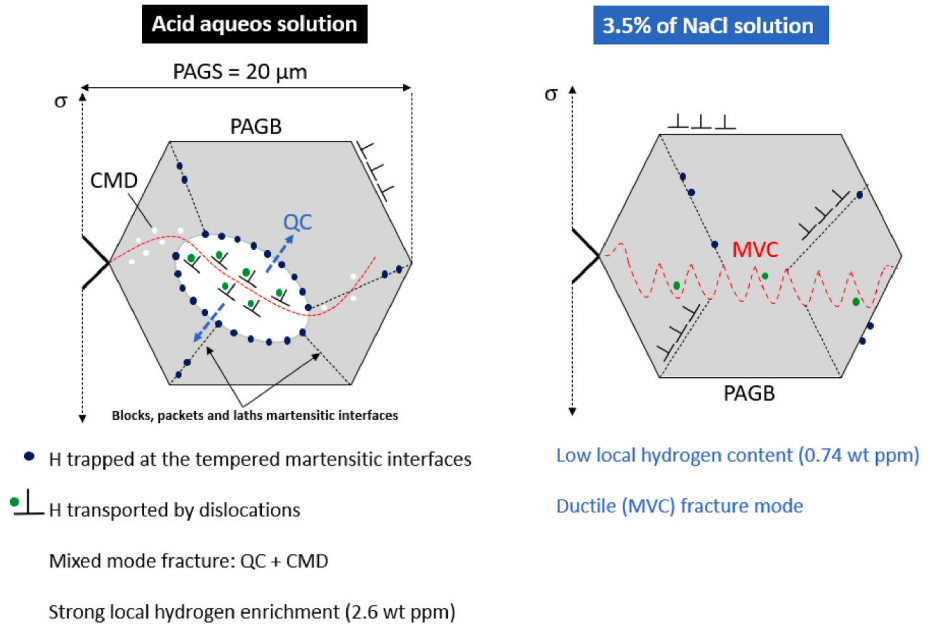

Fig. 15. Fracture micromechanisms in the notched region observed at the maximum embrittlement level (60 MPa/h).

Finally, in order to compare the results obtained in this study with [22], Fig. 16 displays the effect of the prior austenite grain size (PAGS) and hydrogen charging solution in the hydrogen embrittlement susceptibility of a quenched and tempered 42CrMo4 steel submitted to high internal pressure in the presence of internal hydrogen. As can be seen in Fig. 16, hydrogen media play a crucial role in the embrittlement phenomenon and consequently, hydrogen damage has been more pronounced in the high hydrogenated medium (acid solution) when results with PAGS = 20 μm are compared. Additionally, if fracture results are now compared in the acid solution, hydrogen embrittlement has been more marked in the coarser grain steel (PAGS = 150 μm, [22]) what has been also reported by other authors in Refs. [37,42,43].

5. Conclusions

The present study has evaluated the hydraulic fracture behavior at high-internal pressure in the presence of internal hydrogen in a quenched and tempered steel (tempered martensite) after hydrogen precharging in two different solutions: 1 M H_2SO_4 + 0.25 g/l As_2O_3 and 3.5% of NaCl.

By means of the electrochemical hydrogen precharging a higher hydrogen concentration was introduced into the tempered microstructure when the acid solution was employed. Additionally, hydrogen diffusion kinetics at RT was also studied. In this regard, the hydrogen apparent diffusion coefficient and the trapping density sites were estimated to be $3{\cdot}10^{-11}$ m^2/s and $5{\cdot}10^{24}$ sites/m^3, respectively. A binding energy of 45 kJ/mol was calculated from the hydrogen desorption curves data fitting. Results obtained from the hydrogen desorption curves and electrochemical permeation confirm both experimental techniques are adequate to characterize hydrogen uptake and transport.

Hydrogen effect was mainly noted as testing time increased until 1.5 h (60 MPa/h). Besides, hydrogen embrittlement was more marked after hydrogen precharging in the acid solution due to the higher concentration of hydrogen. In this case the burst pressure is reduced of around 19%. Accordingly, important changes on the fracture surfaces were observed. In absence of hydrogen, the fracture micromechanism was totally ductile. However, the fracture micromechanism changes from ductile to quasi-brittle in the presence of internal hydrogen, being this effect especially substantial in the specimens tested at 60 MPa/h. In this case, QC (PRHIC) and CMD micromechanisms, based on HEDE mechanism, were clearly noted near the notch region. On the other hand, fracture micromechanism was always ductile in the samples precharged in 3.5% of NaCl solution, regardless of the loading rate.

Data availability statement

The data that sustain the findings of this study are available from the corresponding author, prior reasonable request.

Declaration of competing interest

The authors declare that they have no known competing financial interests or personal relationships that could have appeared to influence the work reported in this paper.

Acknowledgments

The authors would like to thank the Spanish Government for the financial support received to perform the research projects RTI2018-096070-B-C33 and PID2021-124768OB-C21. This work was also supported by the Regional Government of Castilla y León (Junta de Castilla y León) and by the Ministry of Science and Innovation MICIN and the European Union Next Generation EU/PRTR (MR4W.P2 and MR5W.P3).

References

[1] Matsunaga H, Yoshikawa M, Kondo R, Yamabe J, Matsuoka S. Slow strain rate tensile and fatigue properties of Cr-Mo and carbon steels in a 115 MPa hydrogen gas atmosphere. Int J Hydrogen Energy 2015;40:5739–48. https://doi.org/10.1016/j.ijhydene.2015.02.098.

[2] Peral LB, Zafra A, Fernández-Pariente I, Rodríguez C, Belzunce J. Effect of internal hydrogen on the tensile properties of different CrMo(V) steel grades: influence of vanadium addition on hydrogen trapping and diffusion. Int J Hydrogen Energy 2020;45:22054–79. https://doi.org/10.1016/j.ijhydene.2020.05.228.

[3] Arniella V, Zafra A, Álvarez G, Belzunce J, Rodríguez C. Comparative study of embrittlement of quenched and tempered steels in hydrogen environments. Int J Hydrogen Energy 2022;47:17056–68. https://doi.org/10.1016/j.ijhydene.2022.03.203.

[4] Álvarez G, Arniella V, Belzunce FJ, Rodríguez C. Study of the influence of current density and displacement rate on hydrogen embrittlement using small punch tests. Theor Appl Fract Mech 2023;125:103838. https://doi.org/10.1016/j.tafmec.2023.103838.

[5] Zafra A, Álvarez G, Belzunce J, Rodríguez C. Influence of tempering time on the fracture toughness of hydrogen pre-charged 42CrMo4 steel. Theor Appl Fract Mech 2022;117. https://doi.org/10.1016/j.tafmec.2021.103197.

[6] Zafra A, Peral LB, Belzunce J, Rodríguez C. Effects of hydrogen on the fracture toughness of 42CrMo4 steel quenched and tempered at different temperatures. Int J Pres Ves Pip 2019;171:34–50. https://doi.org/10.1016/j.ijpvp.2019.01.020.

[7] Peral LB, Zafra A, Belzunce J, Rodríguez C. Effects of hydrogen on the fracture toughness of CrMo and CrMoV steels quenched and tempered at different temperatures. Int J Hydrogen Energy 2019;44:3953–65. https://doi.org/10.1016/j.ijhydene.2018.12.084.

[8] Peral LB, Fernández-Pariente I, Colombo C, Rodríguez C, Belzunce J. The Positive role of nanometric molybdenum–vanadium carbides in mitigating hydrogen embrittlement in structural steels. Materials 2021;14:7269. https://doi.org/10.3390/ma14237269.

[9] Zhao H, Wang P, Li J. Effect of vanadium content on hydrogen embrittlement of 1400 MPa grade high strength bolt steels. Int J Hydrogen Energy 2021;46:34983–97. https://doi.org/10.1016/j.ijhydene.2021.08.060.

[10] Frappart S, Feaugas X, Creus J, Thebault F, Delattre L, Marchebois H. Study of the hydrogen diffusion and segregation into Fe–C–Mo martensitic HSLA steel using electrochemical permeation test. J Phys Chem Solid 2010;71:1467–79. https://doi.org/10.1016/j.jpcs.2010.07.017.

[11] Shi R, Chen L, Wang Z, Yang X-S, Qiao L, Pang X. Quantitative investigation on deep hydrogen trapping in tempered martensitic steel. J Alloys Compd 2021;854:157218. https://doi.org/10.1016/j.jallcom.2020.157218.

[12] Sato R, Takai K. Quantitative hydrogen trap states on high-angle grain boundaries and at dislocations in iron. Scripta Mater 2023;228. https://doi.org/10.1016/j.scriptamat.2023.115339.

[13] Briottet L, Moro I, Escot M, Furtado J, Bortot P, Tamponi GM, et al. Fatigue crack initiation and growth in a CrMo steel under hydrogen pressure. In: Int J hydrogen energy, vol. 40. Elsevier Ltd; 2015. p. 17021–30. https://doi.org/10.1016/j.ijhydene.2015.05.080.

[14] Murakami Y, Matsuoka S. Effect of hydrogen on fatigue crack growth of metals. Eng Fract Mech 2010;77:1926–40. https://doi.org/10.1016/j.engfracmech.2010.04.012.

[15] Peral LB, Zafra A, Blasón S, Rodríguez C, Belzunce J. Effect of hydrogen on the fatigue crack growth rate of quenched and tempered CrMo and CrMoV steels. Int J Fatig 2019;120:201–14. https://doi.org/10.1016/j.ijfatigue.2018.11.015.

[16] Shinko T, Halm D, Benoit G, Hénaff G. Controlling factors and mechanisms of fatigue crack growth influenced by high pressure of gaseous hydrogen in a commercially pure iron. Theor Appl Fract Mech 2021;112:102885. https://doi.org/10.1016/j.tafmec.2020.102885.

[17] Colombo C, Fumagalli G, Bolzoni F, Gobbi G, Vergani L. Fatigue behavior of hydrogen pre-charged low alloy Cr-Mo steel. Int J Fatig 2015;83:2–9. https://doi.org/10.1016/j.ijfatigue.2015.06.002.

[18] Sun Z, Benoit G, Moriconi C, Hamon F, Halm D, Hamon F, et al. Fatigue crack propagation under gaseous hydrogen in a precipitation- hardened martensitic stainless steel. Int J Hydrogen Energy 2011;36:8641–4. https://doi.org/10.1016/j.ijhydene.2011.04.094.

[19] Shinko T, Halm D, Benoit G, Hénaff G. Controlling factors and mechanisms of fatigue crack growth influenced by high pressure of gaseous hydrogen in a commercially pure iron. Theor Appl Fract Mech 2021;112. https://doi.org/10.1016/j.tafmec.2020.102885.

[20] Alvaro A, Wan D, Olden V, Barnoush A. Hydrogen enhanced fatigue crack growth rates in a ferritic Fe-3 wt%Si alloy and a X70 pipeline steel. Eng Fract Mech 2019;219. https://doi.org/10.1016/j.engfracmech.2019.106641.

[21] Zafra A, Álvarez G, Benoit G, Henaff G, Martinez-Pañeda E, Rodríguez C, et al. Hydrogen-assisted fatigue crack growth: pre-charging vs in-situ testing in gaseous environments. Materials Science and Engineering: A 2023;871:144885. https://doi.org/10.1016/j.msea.2023.144885.

[22] Peral LB, Díaz A, Arniella V, Belzunce J, Alegre J, Cuesta II. Hydraulic fracture behavior in the presence of hydrogen in notched miniature cylindrical specimens of a 42CrMo4 steel. Eng Fract Mech 2022;274. https://doi.org/10.1016/j.engfracmech.2022.108749.

[23] Zafra A, Belzunce J, Rodríguez C. Hydrogen diffusion and trapping in 42CrMo4 quenched and tempered steel: influence of quenching temperature and plastic deformation. Mater Chem Phys 2020;255. https://doi.org/10.1016/j.matchemphys.2020.123599.

[24] Zafra A, Belzunce J, Rodríguez C, Fernández-Pariente I. Hydrogen embrittlement of the coarse grain heat affected zone of a quenched and tempered 42CrMo4 steel. Int J Hydrogen Energy 2020;45:16890–908. https://doi.org/10.1016/j.ijhydene.2020.04.097.
[25] The adsorption and diffusion of electrolytic hydrogen in palladium. Proc R Soc Lond A Math Phys Sci 1962;270:90–102. https://doi.org/10.1098/rspa.1962.0205.
[26] Peral LB, Amghouz Z, Colombo C, Fernández-Pariente I. Evaluation of hydrogen trapping and diffusion in two cold worked CrMo(V) steel grades by means of the electrochemical hydrogen permeation technique. Theor Appl Fract Mech 2020;110:102771. https://doi.org/10.1016/j.tafmec.2020.102771.
[27] ASTMG148.9789. Standard practice for evaluation of hydrogen uptake, permeation, and transport in metals by an electrochemical technique. 2018.
[28] Peral LB, Díaz A, Alegre JM, Cuesta II. Hydrogen uptake and diffusion kinetics in a quenched and tempered low carbon steel: experimental and numerical study. Int J Hydrogen Energy 2023.
[29] Liu Q, Venezuela J, Zhang M, Zhou Q, Atrens A. Hydrogen trapping in some advanced high strength steels. Corrosion Sci 2016;111:770–85. https://doi.org/10.1016/j.corsci.2016.05.046.
[30] Nagao A, Smith CD, Dadfarnia M, Sofronis P, Robertson IM. The role of hydrogen in hydrogen embrittlement fracture of lath martensitic steel. Acta Mater 2012;60:5182–9. https://doi.org/10.1016/j.actamat.2012.06.040.
[31] Pérez Escobar D, Depover T, Duprez L, Verbeken K, Verhaege M. Combined thermal desorption spectroscopy, differential scanning calorimetry, scanning electron microscopy and X-ray diffraction study of hydrogen trapping in cold deformed TRIP steel. Acta Mater 2012;60:2593–605. https://doi.org/10.1016/j.actamat.2012.01.026.
[32] Moshtaghi M, Loder B, Safyari M, Willidal T, Hojo T, Mori G. Hydrogen trapping and desorption affected by ferrite grain boundary types in shielded metal and flux-cored arc weldments with Ni addition. Int J Hydrogen Energy 2022;47:20676–83. https://doi.org/10.1016/j.ijhydene.2022.04.260.
[33] Yazdipour N, Haq AJ, Muzaka K, Pereloma EV. 2D modelling of the effect of grain size on hydrogen diffusion in X70 steel. Comput Mater Sci 2012;56:49–57. https://doi.org/10.1016/j.commatsci.2012.01.003.
[34] Oudriss A, Fleurentin A, Courlit G, Conforto E, Berziou C, Rébéré C, et al. Consequence of the diffusive hydrogen contents on tensile properties of martensitic steel during the desorption at room temperature. Materials Science and Engineering: A 2014;598:420–8. https://doi.org/10.1016/j.msea.2014.01.039.
[35] Díaz A, Alegre JM, Cuesta II. Numerical simulation of hydrogen embrittlement and local triaxiality effects in notched specimens. Theor Appl Fract Mech 2017;90:294–302. https://doi.org/10.1016/j.tafmec.2017.06.017.
[36] Oriani RA. A mechanistic theory of hydrogen embrittlement of steels. In: Berichte bunsen-ges phys chem. vol. 76; 1972. p. 848–57.
[37] Martiniano GA, Silveira Leal JE, Rosa GS, Bose Filho WW, Piza Paes MT, Franco SD. Effect of specific microstructures on hydrogen embrittlement susceptibility of a modified AISI 4130 steel. Int J Hydrogen Energy 2021;46:36539–56. https://doi.org/10.1016/j.ijhydene.2021.08.147.
[38] Nagao A, Dadfarnia M, Somerday BP, Sofronis P, Ritchie RO. Hydrogen-enhanced-plasticity mediated decohesion for hydrogen-induced intergranular and "quasi-cleavage" fracture of lath martensitic steels. J Mech Phys Solid 2018;112:403–30. https://doi.org/10.1016/j.jmps.2017.12.016.
[39] Huang L, Chen D, Xie D, Li S, Zhang Y, Zhu T, et al. Quantitative tests revealing hydrogen-enhanced dislocation motion in α-iron. Nat Mater 2023. https://doi.org/10.1038/s41563-023-01537-w.
[40] Takeda Y, McMahon CJ. Strain controlled vs stress controlled hydrogen induced fracture in a quenched and tempered steel. Metall Trans A 1981;12:1255–66. https://doi.org/10.1007/BF02642339.
[41] Peral LB, Zafra A, Belzunce J, Rodríguez C. Effects of hydrogen on the fracture toughness of CrMo and CrMoV steels quenched and tempered at different temperatures. Int J Hydrogen Energy 2019;44:3953–65. https://doi.org/10.1016/j.ijhydene.2018.12.084.
[42] Cho L, Bradley PE, Lauria DS, Connolly MJ, Seo EJ, Findley KO, et al. Effects of hydrogen pressure and prior austenite grain size on the hydrogen embrittlement characteristics of a press-hardened martensitic steel. Int J Hydrogen Energy 2021;46:24425–39. https://doi.org/10.1016/j.ijhydene.2021.05.005.
[43] Peral LB, Díaz A, Arniella V, Belzunce J, Alegre JM, Cuesta II. Influence of hydrogen on the hydraulic fracture behavior of a 42CrMo4 steel welds: effect of the prior austenite grain size. Eng Fract Mech 2023;289:109414. https://doi.org/10.1016/j.engfracmech.2023.109414.